Thermal Convection Analysis in a Rotating Shell by a Parallel FEM - Development of a Thermal-Hydraulic Subsystem of GeoFEM -

Hiroaki Matsui [(1)] and Hiroshi Okuda [(2)]

(1) Department of Research for Computational Earth Science, Research Organization for Information Science & Technology (RIST), Tokyo, JAPAN (e-mail: matsui@tokyo.rist.or.jp, Phone: +81-3-3436-5271, fax: +81-3436-5274, (2) Department of Quantum Engineering and System Science, The University of Tokyo, Tokyo, Japan (e-mail: okuda@q.t.u-tokyo.ac.jp, phone: +81-3-5841-7426, fax: +81-3813-3455)

Abstract

We carry out a numerical simulation of thermally driven convection in a rotating spherical shell modeled on the Earth's outer core using Thermal-Hydraulic subsystem of GeoFEM, which gives a parallel FEM platform. This simulation is for understanding of the origin of the geomagnetic field and dynamics of a fluid in the Earth's outer core. We solve a three-dimensional and time dependent process of a Boussinesq fluid in a rotating spherical shell under effects of self gravity and the Coriolis force.In this simulation, tri-linear hexahedron element is applied for spatial distribution, and 2nd-order Adams-Bashforth scheme are applied for time integration of the temperature and velocity. To satisfy the mass conservation, a parallel iterative solver of GeoFEM is applied for solving pressure and correction of the velocity fields. To verify our simulation code, results of the simulation are compared with the same analysis by the spectral method. In these results, outline of convection is almost same in these cases; that is, three pairs of convection columns are formed, and these columns propagate to the westward in quasi-steady state. However, magnitude of kinetic energy averaged over the shell is about 93% of that in the case by the spectral method, and drift frequency of the columns in the GeoFEM case is larger than that in the case by the spectral method.

1. Introduction

It has been widely accepted that the geomagnetic field is generated by motion of an electrically conductive fluid in the Earth's outer core. This cause is referred as "dynamo process." The motion of the fluid in the outer core is strongly influenced by the Lorentz force and the Coriolis force which, in the co-rotating frame, is given by, $-2\rho\boldsymbol{\Omega} \times \boldsymbol{v}$, where ρ, $\boldsymbol{\Omega}$, and $\boldsymbol{v}$ are density of the fluid, angular velocity of the Earth's rotation, and velocity of the fluid, respectively. Furthermore, the dynamo process is not only complicated nonlinear system, but also requires three-dimensional and time dependent treatment for direct simulations. In the last five years, the investigation of the generation processes of the Earth and planetary magnetic fields has entered into a new stage; several MHD simulations in a rotating spherical shell have represented some of the basic characteristics of the Earth's magnetic field after Glatzmaier and Roberts (1995a[7], 19995b[8]) and Kageyama et.al. (1995[11]). After these studies, many studies of the geodynamo simulation represent strong and dipole like magnetic fields by which geomagnetic field is characterized (Kuang and Bloxham, 1997[12], 1999[13]; Christensen, 1999[4], Sakuraba (1999)[15]). Most of these simulations, however, have been

applied the spherical harmonics expansion in the azimuthal and elevation directions, because high spectral accuracy is obtained in this method, singularity of physical values is kept at poles, and magnetic fields are easily connected to potential field on the boundaries. Only in the cases by Kageyama et. al. (1995)[11] the finite difference method is applied, while they have considered a compressible gas for a model of the fluid and applied a different magnetic boundary condition at outer boundary of the shell from the condition estimated at the Earth's Core-Mantle boundary. The spectral harmonics expansion which is the general scheme for the geodynamo simulation is, however, not suitable for the massively parallel computation because a lot of global calculation is required to solve nonlinear terms. On the other hand, Finite Element Method (FEM) is suitable for massively parallel computation because of their local operation. If we set an extremely large scale FEM mesh, we can carry out large scale simulation for the motion in a rotating spherical shell in massively parallel computers. We are developing a simulation code for MHD simulation in a rotating spherical shell for understanding the geodynamo process and dynamics of a fluid in the shell using GeoFEM [6], which gives a parallel FEM platform for solid Earth simulation. Now, we have developed a simulation code for thermal convection in a rotating flame without magnetic field and carry out numerical simulations of the thermal convection in the rotating spherical shell. This results are compared with the simulation results by the spectral harmonics expansion. In this study, we compare the simulation results with that by a simulation using the spherical harmonics expansion to investigate whether same results are obtained by these simulations or not. The results shows that 3 pairs of convection column which parallel with respect to the rotation axis are generated and these columns propagate to the westward in both cases in quasi-steady state. In detail, some differences are seen in these results; that is, magnitude of kinetic energy is about 93% to that in the case by the spectral method, and drift frequency of the convection pattern is faster than that in the case by the spectral method. This paper consists of the following sections: In section 2, we describe a model for this simulation and method of the simulation for the two cases. Results of the simulations are given in Section 3. In Section 4, we make a discussion about these results. In Section 5, conclusion is described.

2. Simulation Model and Methods

Model for this simulation

We consider a rotating spherical shell modeled on the Earth's outer core as given in Fig.1. Ratio of the inner boundary to outer boundary of the spherical shell is set to be 0.4 while the ratio of the Earth's outer core is to be 0.35. The shell is filled a Boussinesq fluid and rotate with a uniform angular velocity $\mathbf{\Omega}$. The fluid has constant thermal diffusivity κ, kinetic viscosity ν, and thermal expansion coefficient α. We assume that the inner core co-rotate with the mantle to simplify the model. Motion of the fluid in a rotating flame is described by the mass conservation, the momentum equation (Navier-Stokes equation) with the Boussinesq approximation and with the Coriolis term, and the thermal diffusion equations; that is,

$$\mathrm{div}\, \boldsymbol{v} = 0, \tag{1}$$

$$\frac{\partial \boldsymbol{v}}{\partial t} + (\boldsymbol{v}\cdot\nabla)\,\boldsymbol{v} = -\nabla P + P_r\nabla^2\boldsymbol{v} - P_r\sqrt{T_a}\,(\mathbf{\Omega}\times\boldsymbol{v}) + P_r R_a \Theta \boldsymbol{r}, \tag{2}$$

$$\frac{\partial \Theta}{\partial t} + (\boldsymbol{v}\cdot\nabla)\,(\Theta + T_0) = \nabla^2\Theta, \tag{3}$$

$$T = \Theta + T_0, \text{ and} \tag{4}$$

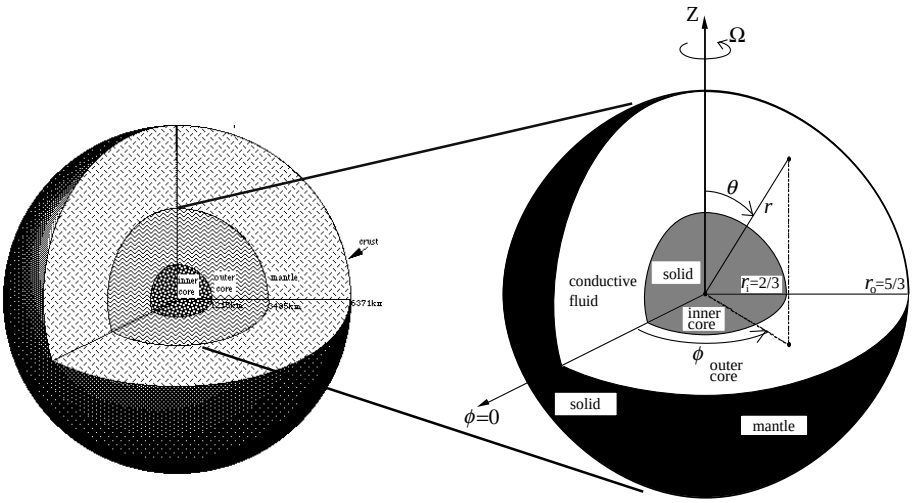

Figure 1: Rotating spherical shell modeled on the Earth's outer core. Sketch of the Earth's interior are given in the left panel, and the rotating spherical shell model is given in the right panel.

$$T_0 = \frac{r_i r_o - r_i r}{r\left(r_o - r_i\right)}, \tag{5}$$

where, $\boldsymbol{v}$, P, $\boldsymbol{\Omega}$, $\boldsymbol{r}$, Θ, T_0, r_o, and r_i are velocity, modified pressure, vector of the Earth's rotation, position vector, perturbation of temperature, reference temperature, radius of the outer boundary of the shell, and radius of the inner boundary of the shell, respectively. To obtain above normalized equations, we choose width of the shell $L = r_o - r_i$, thermal diffusion time L^2/κ, as the length scale and time scale, respectively. There are three dimensionless numbers in above equations; that is, the Prandtl number P_r, the Rayleigh number R_a , and the Taylor number T_a; These numbers are given by,

$$P_r = \frac{\nu}{\kappa}, \tag{6}$$

$$R_a = \frac{g\alpha\Delta T L^3}{\kappa\nu}, \text{ and} \tag{7}$$

$$T_a = \left(\frac{2\Omega L^2}{\nu}\right)^2, \tag{8}$$

where ν, κ, α, ΔT, and g are the kinetic viscosity, the thermal diffusivity, the thermal expansion ratio, and difference of temperature between the inner and outer boundaries f the shell. In the Earth's outer core, The Taylor number and the Rayleigh number are estimated to be $T_a = 10^{30}$ and $R_a = 6 \times 10^{30}$ with the molecular viscosities (Gubbins, 1987[9]). Even if we consider turbulent viscosities, these dimensionless number stays more than 10^{10}. We cannot set these dimensionless numbers to be these estimated values directly because of limitation of computational power. Then, we set the Prandtl number to be 1, with Taylor number to be 2.5×10^5, and the Rayleigh number to be $1.5 \times 10^4 = 1.8 R_{ac}$, where R_{ac} is the critical Rayleigh number.

Boundary conditions have strongly effects to the motion of the fluid. In this study, we choose the rigid boundary condition for the velocity and fixed temperature for the temperature boundary conditions at the both boundary conditions; that is,

$$\boldsymbol{v} = 0 \qquad \text{at } r = r_o,\, r_i\ , \tag{9}$$

$$\boldsymbol{T} = 1 \qquad \text{at } r = r_i, \text{ and} \tag{10}$$
$$\boldsymbol{T} = 0 \qquad \text{at } r = r_o. \tag{11}$$

Methods of the simulation in the case by GeoFEM

Our simulation code is based on GeoFEM Thermal-Hydraulic subsystem, which is for numerical simulations of thermally driven convection by parallel Finite Element method (FEM). In this subsystem, the basic equations eqs. (1) - (3) for the fluid are solved three dimensionally and time independently. The spherical shell is divided into tri-linear hexahedron elements, and the temperature, velocity, and pressure are defined at each node and interpolated by tri-linear function in each hexahedron element. For the time integration, we apply the fractional step scheme and Adams-Bashforth scheme to obtain high accuracy for the Coriolis term. Process of the simulation is given in the following equations; that is,

$$\bar{M}_{\alpha\beta}\Theta_\beta^{n+1} = \bar{M}_{\alpha\beta}\Theta_\beta^n + \Delta t\left(\frac{3}{2}F_T^n - \frac{1}{2}F_T^{n-1}\right), \tag{12}$$
$$\bar{M}_{\alpha\beta}\tilde{v}_{i\beta} = \bar{M}_{\alpha\beta}v_{i\beta}^n + \Delta t\left(\frac{3}{2}F_{vi}^n - \frac{1}{2}F_{vi}^{n-1}\right), \tag{13}$$
$$\frac{1}{\Delta t}\left(-L_{\alpha\beta} + S_{\alpha\beta}\right)\Phi_\beta = H_{\alpha\beta}^i\tilde{v}_{i\beta}, \tag{14}$$
$$P_\alpha^{n+1} = \frac{1}{\Delta t}\Phi_\alpha, \text{ and} \tag{15}$$
$$\bar{M}_{\alpha\beta}v_{i\beta}^{n+1} = \bar{M}_{\alpha\beta}\tilde{v}_{i\beta} + H_{\alpha\beta}^i\Phi_\beta, \tag{16}$$

where the diffusion, inertia, and forces terms are given by,

$$F_T^n = \left\{\left(-L_{\alpha\beta} + S_{\alpha\beta}\right)\Theta_\beta^n - H_{\alpha\beta}^j v_{ej}^n\left(\Theta_\beta^n + T_{0\beta}\right)\right\}, \text{ and} \tag{17}$$
$$F_{vi}^n = \Big\{P_r\left(-L_{\alpha\beta} + S_{\alpha\beta}\right)v_{i\beta}^n - H_{\alpha\beta}^j v_{ej}^n v_{i\beta}^n - P_r T_a^{1/2} e_{ijk} M_{\alpha\beta}\Omega_{j\alpha}v_{k\beta} - P_r R_a M_{\alpha\beta}\Theta_\beta^{n+1}g_i\Big\}, \tag{18}$$

In above equations, e_{ijk} is the permutation symbol, and v_{ei} is velocity averaged over each element; that is,

$$v_{ei} = \sum_{\alpha=1}^{8} v_{i\alpha}\frac{1}{V_e}\int_{\Omega_e} N_\alpha dV. \tag{19}$$

Each component of matrix $M_{\alpha\beta}$, $\bar{M}_{\alpha\beta}$, $L_{\alpha\beta}^i$, $H_{\alpha\beta}^i$, $S_{\alpha\beta}^i$ in eqs.(12)-(17) are described following integrations, that is,

$$M_{\alpha\beta} = \int_{\Omega_e}\tilde{N}_\alpha N_\beta dV, \tag{20}$$
$$\bar{M}_{\alpha\beta} = \left[\sum_\beta M_\alpha\beta\right]\delta_{\alpha\beta}, \tag{21}$$
$$L_{\alpha\beta} = \int_{\Omega_e}\frac{\partial N_\alpha}{\partial x_i}\frac{\partial N_\beta}{\partial x_i}dV, \tag{22}$$
$$H_{\alpha\beta}^i = \int_{\Omega_e}\tilde{N}_\alpha\frac{\partial N_\beta}{\partial x_i}dV, \text{ and} \tag{23}$$
$$S_{\alpha\beta} = \oint_{\Omega_e}\tilde{N}_\alpha\frac{\partial N_\beta}{\partial x_i}n_i dS, \tag{24}$$

where, N_α is tri-linear shape function, and up-winded shape function $\tilde{N}_\alpha$ is defined as,

$$\tilde{N}_\alpha = N_\alpha + \frac{\Delta t}{2} v_{ej} \frac{\partial N_\alpha}{\partial x_j}. \tag{25}$$

First, temperature at the next step is solved by eq.(12) with eq.(18). Then, to obtain predictor of the velocity $\tilde{v}_i$ eq.(13) with eq.(17) are solved. To satisfy the mass conservation low, divergence of the predictor is calculated and Poisson equation eq. (14) are solved by the parallel CG solver of GeoFEM. Then pressure p^{n+1} and velocity v_i^{n+1} are solved by eqs.(15) and (16).

The spherical shell is divided into tri-linear finite elements. The finite element mesh is generated by the following process: We consider an icosahedron and this icosahedron is refined three times. Next, to obtain a hexahedral element, each triangle is devide into three quadrilaterals. Finally, this mesh is stacked in the radial direction. In this study, the spherical shell is divided into 33 layers including both boundaries in the radial direction and 3842 nodes are set on each sphere surface. Distance of nodes are about 70 km in the radial direction and about 3 degree in the longitudinal direction at the equator. For parallel computation, domain decomposition method has been applied in GeoFEM. The finite element mesh is divided into 32 domains in this study. This partitioning is carried out a partitioner of GeoFEM to parallel with respect to x, y, and z planes and to balance the number of nodes in each domain. In Fig.2, the grid pattern of the spherical shell is given.

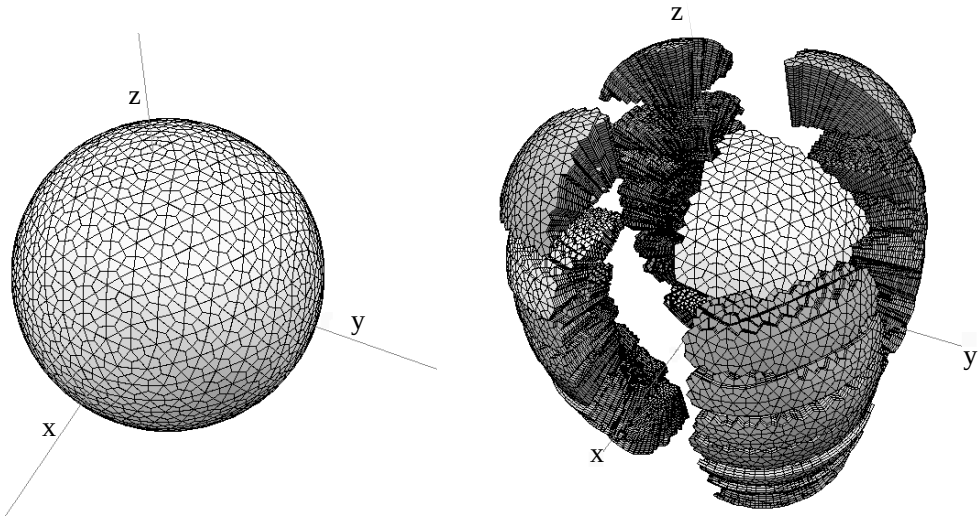

Figure 2: Grid pattern for the rotating spherical shell. Grid pattern for whole spherical shell is given in the left panel, and distributed grid pattern for parallel computation are given in the right panel.

Simulation method in the case by the spectral method

To verify results of the simulation by GeoFEM, we carry out the same simulation by the spectral method. In this case, the simulation scheme is based after Frazer (1974[5]), Honkura and Matsushima (1992[10]), and Matsui (1999[14]). It is well established that arbitrary solenoidal vector fields can be separated into poloidal and toroidal components (Bullard, 1954[1]; Chandrasekhar, 1961[3]). The velocity field is solenoidal because we apply the Boussinesq approximation in the present study. Scalar functions of the poloidal velocity V_S and toroidal velocity

V_T and temperature perturbation are expanded into the spherical harmonics; that is,

$$\boldsymbol{v} = \text{rot rot } (V_T\boldsymbol{r}) + \text{rot } (V_T\boldsymbol{r}) \tag{26}$$

$$V_S(\boldsymbol{r},t) = \sum_{l=1}^{L}\sum_{m=-l}^{l} {V_{Sl}}^m(r,t)Y_l^m(\theta,\phi) \tag{27}$$

$$V_T(\boldsymbol{r},t) = \sum_{l=1}^{L}\sum_{m=-l}^{l} {V_{Tl}}^m(r,t)Y_l^m(\theta,\phi) \tag{28}$$

$$\Theta_(\boldsymbol{r},t) = \sum_{l=0}^{L}\sum_{m=-l}^{l} {\Theta_l}^m(r,t)Y_l^m(\theta,\phi) \tag{29}$$

where, $Y_l^m(\theta,\phi)$ and L are the spherical harmonics and its truncation level, respectively. We solve the coefficients of the harmonics ${V_{Sl}}^m$, ${V_{Tl}}^m$, and ${\Theta_l}^m$. To find solution in the radial direction, we apply the 2nd order finite difference method. In this case, we solve the heat conduction equation and the vorticity equation for the poloidal and toroidal component of the vorticity. The poloidal velocity is obtained by the toroidal vorticity using the Poisson equation. To solve the time evolution, we adopt the Crank-Nicolson scheme for the diffusion terms and 2nd-order Adams-Bashforth scheme for solving the other terms. It is noted that the inertia terms and the Coriolis term are solved by the coefficients of the spherical harmonics. Because amount of computation increases $O(L^5)$ order in this scheme, it is difficult to apply large truncation level. In this study, truncation level of the spherical harmonics is set to be 18 degree with equally divided 64 grid points in the radial direction.

These simulations are carried out the following computers; the simulation by GeoFEM is carried out 4 nodes of Hitachi SR8000 in Information Science Center of National Institute of Polar Research. The case has been carried out by NEC SX-4/128H in Computer Center, Tohoku University in the case by the spectral method.

3. Results of the Simulation

We compare with three points of the results of the simulation by GeoFEM with that by the spectral method; that is, i) time variation of the convection pattern, ii) kinetic energy and z-component of angular momentum averaged over the spherical shell, and iii) time variation of the convection pattern.

Convection pattern

After Busse (1970[2]), many analytical studies and numerical simulations have been shown that columnar convection which parallel with respect to the rotation axis are formed outside of the tangential cylinder, which is a imagimally cylinder attached to the inner boundary of the shell at equator, in the case of thermally driven convection in a rotating spherical shell. To show characteristics of the convection pattern in a quasi-steady state, isosurface of $P = 1000$ and $P = -1000$ and contour map of z-component of vorticity $\omega_z = \text{rot } \boldsymbol{\omega}\hat{z}$ in a cross section at $z = 0.35$ are shown in Fig.3. In this simulation, three pairs of convection columns which parallel with respect to the rotation axis are formed. As shown in Fig.3, convection columns with low pressure have positive z-component of vorticity and vice varsa. In upper panels of Fig.4, intensities of the z-component of the vorticity and of the velocity at the cross section of $z = 0.35$ are given. In the convection columns, z-component of the velocity and vorticity have opposite direction; i.e., the clockwise vortices have the poleward flow, while the counterclockwise vortices have the equatorward flow. These structures of the convection are

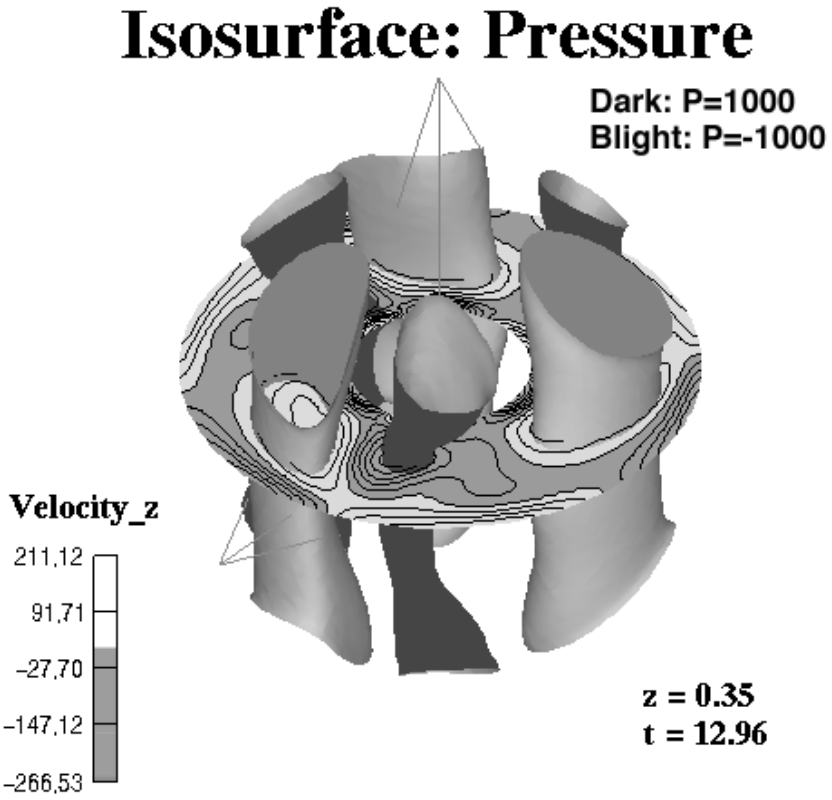

Figure 3: Convection pattern at $t = 12.96$ for the simulation by GeoFEM. Pressure is shown as isosurfaces of $P = -1000$ (dark surface) and $P = 1000$ (blight surface). Intensity of z-component of the vorticity at a cross section of $z = 0.35$ is given by a contour map. Regions which have negative vorticity are filled gray in the contour map.

characterized as helical flows. To verify that this simulation works correctly, we compare this convection pattern with convection pattern for the case by the spherical harmonics expansion. Z-compoenet of vorticity and velocity at the same cross section as the case by GeoFEM are shown in the lower panels of Fig.4. As seen in these figures, the convection patterns are almost same except for posision of the each convection column. Intensity of the velocity in the case of GeoFEM is, however, smaller than that by the spectral method. This difference is also seen in the magnitude of the kinetic energy averaged over the spherical shell.

Averaged kinetic energy and angular momentum

Time evolution of kinetic energy averaged over the spherical shell, which is defined by $\frac{1}{V}\int \frac{1}{2}v^2 dV$ is given in Fig.5. Comparing between these two cases, time evolutions are different between two cases in $t < 7$. After $t = 11$, however, the behaviors of the kinetic energy become quite similar to each other. This difference in the beginning of the simulations is caused by difference of initial temperature between two cases; that is, in the case of GeoFEM, we set initial temperature to be $T = 1$ on the inner boundary and to be $T = 0$ the other region, while small temperature perturbation is given in the all mode of the spherical harmonics as initial temperature for the case by the spectral method. After $t = 11$, the kinetic energy in both cases shows similar changes because effects of the initial temperature vanish. The

GeoFEM

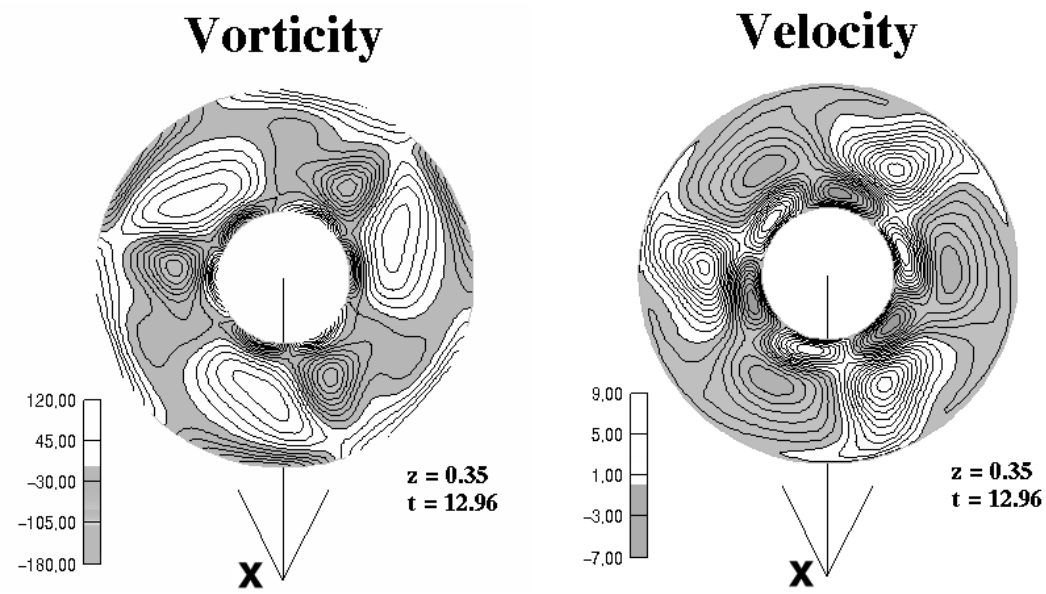

Spectral method

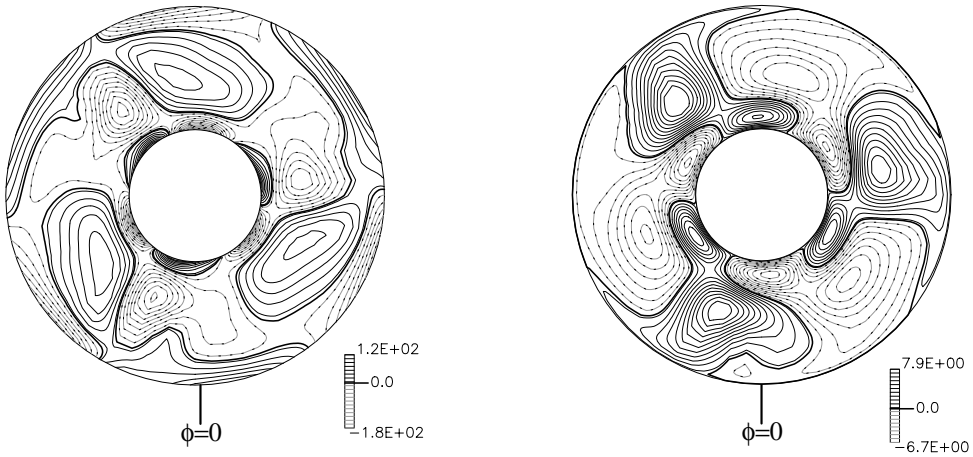

Figure 4: Intensity of the z-component of vorticity (left panels) and velocity (right panels) at a cross section of $z = 0.34$ at a quasi-steady state. The results for the simulation by GeoFEM at $t = 12.96$ are given in left panels, and the results at $t = 12.0$ for the simulation by the spectral method are given in the right panels. Range of the vorticity is from -180.0 to 120.0 for both cases, and that of the velocity is from -6.7 to 7.9 for the case by the Spectral method and from -7.0 to 9.0 for the case by the GeoFEM.

magnitude of the kinetic energy is, however, different between the two cases. The averaged kinetic energy and z-component of the angular momentum $\frac{1}{V}\int (\boldsymbol{r} \times \boldsymbol{v})\, dV$ at quasi-steady state are given in Table . In $t > 11$, magnitude of the kinetic energy for the case by GeoFEM is about 93% of that in the case by the spectral method. On the other hand, z-component of

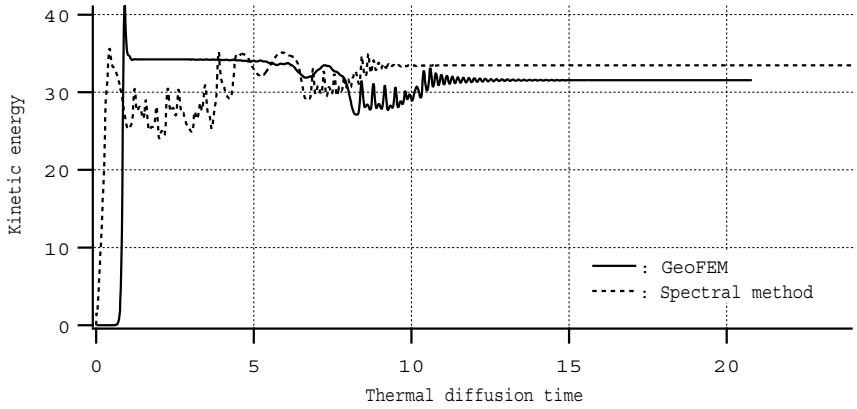

Figure 5: Time evolution of kinetic energy averaged over the spherical shell. The energy for the case by GeoFEM is given by the solid line, and that by the spectral method are given by the dotted line.

	GeoFEM	Spectral method
Kinetic energy	31.6	33.5
Angular momentum	-0.919	-0.849
drift frequency	-1.88	-1.62

Table 1: Kinetic energy and angular momentum averaged over the spherical shell and drift frequency of the convection pattern at $t = 18.0$. Positive value of the drift velocity is defined as eastward propagation.

angular momentum averaged over the shell is larger than that by the spectral method. This results suggest that details of convection patterns are also different between these cases.

Time variation of convection patterns

As many simulation results are shown, convection patterns are propagate in the longitudinal directions as described by

$$(\boldsymbol{v}, \Theta) = \boldsymbol{f}(r, \theta, \phi - \omega t)\,, \tag{30}$$

where ω is drift frequency. To investigate variations of the convection patterns and to estimation the drift frequency of the convection, we plot radial velocity at mid-depth of the shell and the equatorial plane as given in Fig 6. As shown in Fig.6, convection patterns propagate to the westward throughout these simulations, and the number of the convection columns changes from 4 pairs to 3 pairs in $7.0 < t < 10.0$. The drift frequency becomes almost constant in $t > 11$, but the drift frequency is different between these simulations. To estimate the drift frequency, we choose a component of the radial velocity described as $v_r(t)\cos(3\phi - \omega t)$. The drift frequency in the quasi-steady state is estimated by phase of a wave of this component of the velocity, and the drift frequency is plotted as a function of time in Fig.7. As given in Fig.7, magnitude of the drift frequency is larger than that in the case by the spectral method; i.e., the convection pattern for the case by GeoFEM propagates rapidly in the case by GeoFEM. As given in Table the magnitude of the drift frequency in quasi-steady state is 1.13 times to that for the case by the Spectral method.

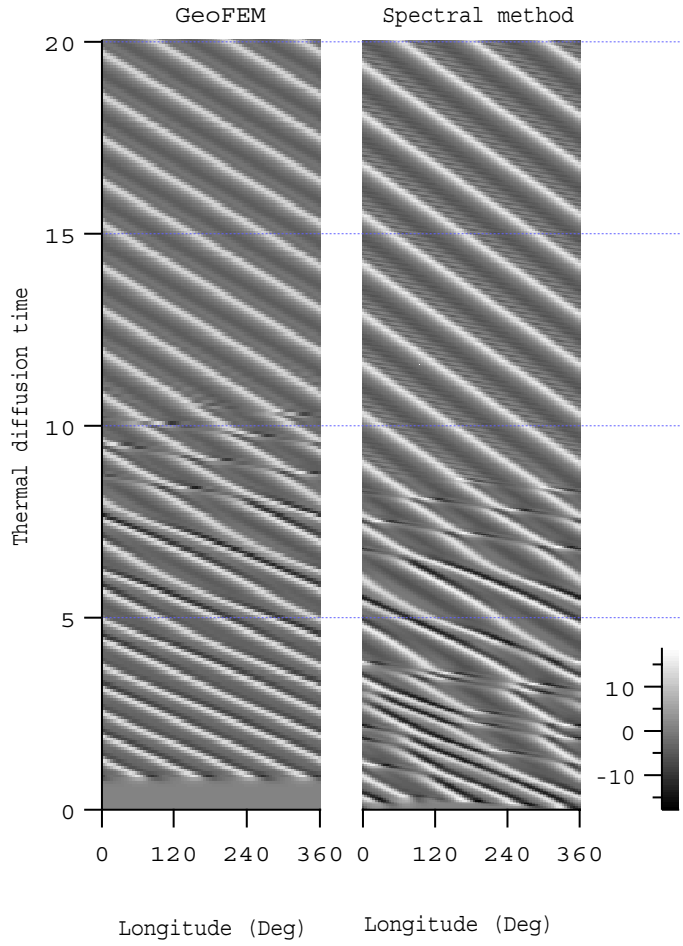

Figure 6: Radial velocity v_r along a circle made at equatorial plane and mid-depth of the shell as functions of the longitude (horizontal axis) and time (vertical axis). This figure is for displaying propagation of the convection pattern in the zonal direction. The result for the case by GeoFEM is given in the left panel, and that for the case by the spectral method are given in the right panel. Positive value means outward flows, and positive values are shown by white and negative values are shown by black. Range of grayscale is from -17.5 to 18.5.

4. Discussion

Our simulation results by GeoFEM and that by the spectral harmonics expansion show the similar convection pattern and time variations of in qualitatively. As seen in Table , however, about 10% of differences are seen several values are seen in the results. These two simulations have many differences; that is, spatial resolution, radial resolution, and initial temperatures. In these differences, The resolution of the radial direction may cause serious problems in our results. In both cases, the radial resolution affects the convection patterns around the both boundaries because radial resolution is too low to describe boundary layers. This error in the case by GeoFEM may be larger than that by the spherical harmonics expansion, because the radial resolution in the case by GeoFEM is lower than that by the spectral method. However, when we set the larger number of nodes in radial direction, length of times step has to set to be much shorter. In fact, we carry out this simulation with a grid which has 64 nodes in the radial direction and has the same mesh pattern in a sphere as the simulation described in Section 3. In this case, we set the time step to be 0.1 times to the previous

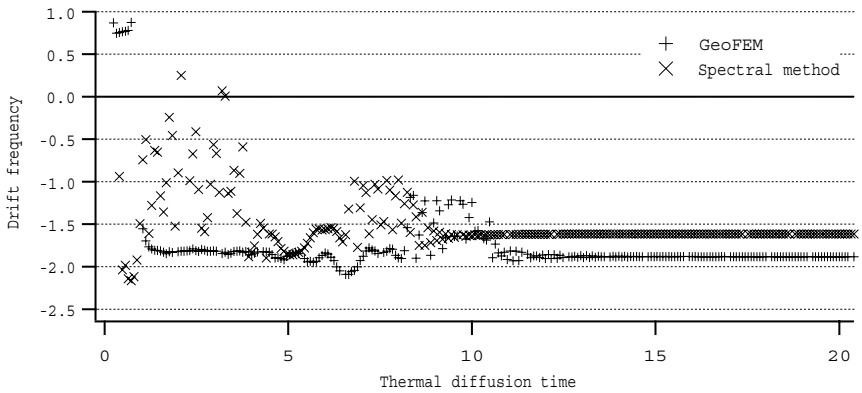

Figure 7: Angular drift frequency of the radial component of the velocity with three wave numbers in the longitudinal direction along a circle made at equatorial plane and mid-depth of the shell as a function of thermal diffusion time. This drift frequency is shown the drift frequency of the convection patterns after $t = 11$ because three pairs of convection columns are formed after $t = 11$. The result for the case by GeoFEM is plotted by "+", and that for the case by the spectral method is given by "$\times$." Positive drift velocity means that convection pattern drift to the eastward.

case. Because CPU time for this case is 20 times longer than that for the simulation given in Section 3. We carry out this simulation only to $t = 4.5$. This simulation seems to be reaches the quasi-steady state rapidly than the last case (see Fig.8 and Fig.9). Magnitude of averaged kinetic energy and angular momentum in this case reaches to be 32.7 and -0.866, respectively. There is only 3% of difference between the result by GeoFEM and that by the spectral method.

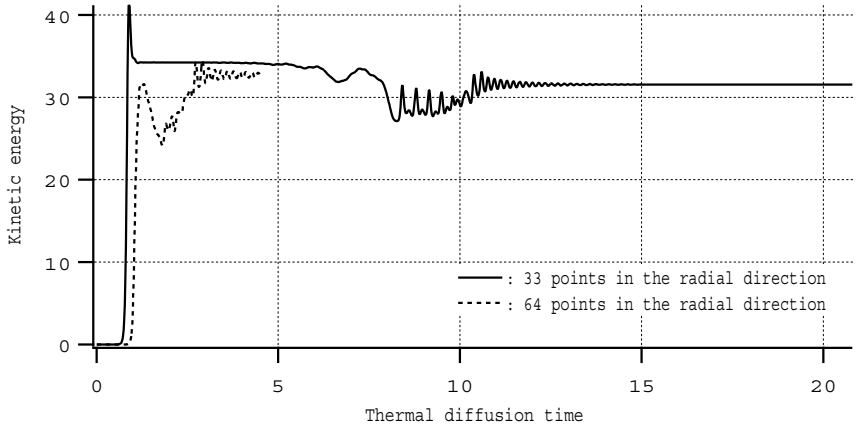

Figure 8: Time evolution of kinetic energy averaged over the spherical shell for the cases by GeoFEM. Results by the mesh with 33 layers are given by the solid line (same as Fig.5), and that by the mesh with 64 layers are given by dotted line.

Because of this reason, we have to carry out this simulation with much higher resolution especially at around both of boundaries. This requires much shorter time steps for this simulation. It is a large problem how fast this simulation can carry out. Elapse time for time evolution in the simulations shown in Section 3 is estimated as shown in table .

It is not important to compare these elapse time by GeoFEM with that by the spectral method directly because these simulations have different spatial resolutions, methods and

33 layers in the radial direction 64 layers in the radial direction

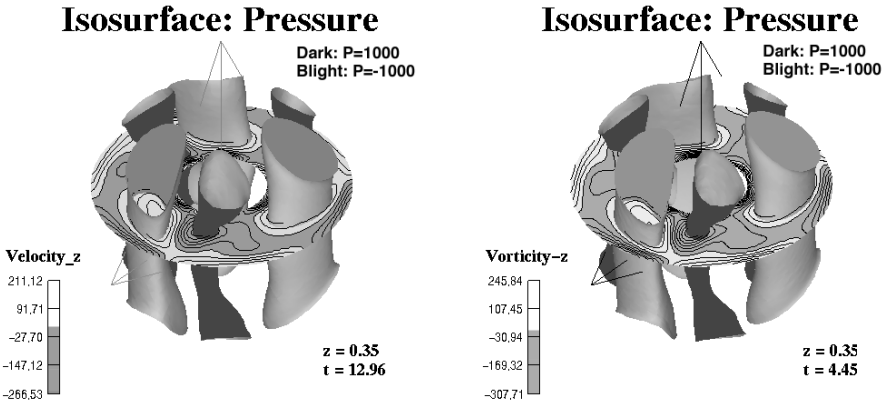

Figure 9: Convection pattern at $t = 12.96$ for the case with 33 layers in the radial direction (left panel) and that at $t = 4.45$ for the case with 64 layers in the radial direction (right panel). Format of Figures are same as Fig.3, and the figure in the left panel is the same as Fig.3.

Method	Machine	elapse time for 100 steps
GeoFEM	SR8000(8PEs)	1202
GeoFEM	SR8000(16PEs)	830.5
GeoFEM	SR8000(32PEs)	434.8
Spectral method	SX-4(16PE)	33.3

Table 2: Elapse times for 100 time steps of the simulation.

machines where we have carried out these simulations. However, it is noted that we have to carry out a MHD simulation about 10 times longer time steps than that of this simulations when we set the same parameters for the fluid for the MHD dynamo simulation in this shell. In this study, we carry out 2×10^5 time steps in these simulations, then it takes about 250 hours to obtain the simulation results at t = 20.0 while it takes only for 22 hours in the case by the Spectral method. If we carry out MHD simulation with same FEM mesh, same time steps, and same machines, it will take about 5000 hours to obtain results of the MHD dynamo simulation. However, because our simulation code provides about only 5% of the peak performance of SR8000, there are a lot of modification points to obtain efficiency of the simulation.

5. Conclusion

For understanding of the dynamics of a fluid in the Earth's outer core, we have been developing a simulation code for the fluid motion in a rotating spherical shell modeled on the Earth's outer core. This code is based on Thermal-Hydraulic subsystem of GeoFEM, which gives a parallel FEM platform. As a developing processes, we carry out a simulation of thermally driven convection in the rotating spherical shell without magnetic field. In this simulation,

tri-linear hexahedron elements are applied for spatial distribution, and the spherical shell is divided into 33 layers including both boundaries and 3842 nodes are set with a refined icosahedral pattern on each spherical surface. This Finite Element mesh is divided into 32 domains for the parallel computation by a partitioner provided by GeoFEM. For time evolution of the temperature and velocity by the inertia, buoyancy, and Coriolis force, 2nd-order Adams-Bashforth scheme are applied. Pressure is solved by parallel CG solver of GeoFEM. In the simulation by the spectral method, poloidal and toroidal component of velocity and temperature are expanded into the spectral harmonics expansion in the azimuthal and elevation direction, and the finite difference method is applied in the radial direction. For the time integration, we apply the Crank-Nicolson scheme for diffusion terms and Adams-Bashforth scheme for the other terms. Because dimensionless numbers for the Earth's core such as the Rayleigh number and the Taylor number is too large to be applied to the simulation, we choose these parameters in the range which we can carry out the simulation; that is, the Prandtl number is set to be 1.0, and the Taylor number is set to be 2.5×10^5 with the Rayleigh number of $1.5 \times 10^4 = 1.8 R_{ac}$, where R_{ac} is the critical Rayleigh number. The rigid boundary is set on the inner and outer boundaries as a boundary condition for velocity, and temperature is set to be 1 on the inner boundary and set to be 0 on outer boundary as a temperature boundary condition. We carry out these simulations to 20 times of thermal diffusion time.

The results of the convection pattern show that three pairs of convection columns which parallel with respect to the rotation axis are dominantly formed and that these columns propagate to the westward in the quasi-steady state of the simulation. Although different initial values of the temperature are set in these two cases, same characteristics of the convection are obtained in the two cases. On the other hand, the kinetic energy in the shell is about 93% of that in the case using the spectral method, and the magnitude of drift frequency of the convection pattern is 1.13 times larger than that for the simulation by the Spectral method. We consider that this discrepancy is mainly caused by difference of the spatial resolution in the radial direction.

To investigate the Earth's core dynamics and the geodynamo process, We have to simulate the motion of the fluid magnetohydrodynamically. Thus, development of a MHD code based on this subsystem is deferred for the further studies. At the same time, some modification is required to obtain an efficiency of computation.

Acknowledgement

This study is a part of the project "Solid Earth Platform for Large Scale Computation" funded by the Ministry of Education, Culture, Sports, Science and Technology, Japan through its "Special Promoting Funds of Science & Technology."

Furthermore, the authors would like to thank Prof. Yoshi-yuki Hayashi (Hokkaido University), Dr. Shin-ichi Takehiro (Kyushu University), Dr. Masaki Matsushima (Tokyo Institude of Technology) and Mr. Muga Nakanishi (Tokyo Institude of Technology) for frouitful discussions with the understanding for the simulation results, Dr. Masaki Okada for his helpful advice for uisng Hitachi SR8000 system in Information Science Center, Natinal Institute of Polar Research, and collagues in GeoFEM project for hearty support for this study.

References

[1] Bullard, E. C. and H. Gellman, Homogeneous dynamos and terrestrial magnetism *Phil.*

Trans. Roy. Soc. Lond., **A247**, 213-278, 1954.

[2] Busse, F.H., Thermal instabilities in rapidly rotating systems *J. Fluid Mech.,* **44**, 441-460, 1970.

[3] Chandrasekhar, S., Hydrodynamic and Hydromagnetic Stability, Oxford University Press, 1961.

[4] Christensen, U., P. Olson and G.A. Glatzmaier, Numerical modelling of the geodynamo: a systematic parameter study, *Geophys. J. Int.* , **138**, 393-409,1999.

[5] Frazer, M.C., Spherical hermonic analysis of the Navier-Stokes equation in magnetofluid dynamics, *Phys. Earth Planet Inter.*, **8**, 75-82,1974.

[6] GeoFEM Web Site: http//www.geofem.org

[7] Glatzmaier, G.A. and P.H. Roberts, A three-dimensional self-consistent computer simulation of a geomagnetic field reversal, *Nature* , **377**, 203-209, 1995a.

[8] Glatzmaier, G.A. and P.H. Roberts, A three-dimensional convective dynamo solution with rotating and finitely conducting inner core and mantle, *Phys. Earth Planet. Inter.* , **91**, 63-75, 1995b.

[9] Gubbins, D. and P.H. Roberts, Magnetohydrodynamics of the Earth's Core in Geomagnetism vol.2, pp.1-183, Academic Press, 1987

[10] Kageyama, A., T. Sato and the Complexity Simulation Group, Computer simulation of a magnetohydrodynamic dynamo, *Phys. Plasmas*, **44**, 931-941, 1992.

[11] Honkura, Y., T.Iijima and M. Matsushima, Magnetic field reversal resulting from a dynamo process in a spherical shell, *J. Geomag. Geoelectr.*, **2**, 1421-1431, 1995.

[12] Kuang, W. and J. Bloxham, An Earth-like numerical dynamo model, *Nature*, **389**, 371-374, 1997.

[13] Kuang, W. and J. Bloxham, Numerical modeling of magnetohydrodynamic convection in a rapidly rotating spherical shell: weak and strong field dynamo action, *J. Comput. Phys.*, **153**, 51-81, 1999.

[14] Hiroaki Matsui, Studies on the Basic Processes of Magnetic Field Generation Based on MHD Simulation in the Rotating Spherical Shell, Ph.D. Thesis, Tohoku Univ.,1999.

[15] Sakuraba, A. and M. Kono, Effects of the inner core on the numerical simulation of the magnetohydrodynamic dynamo*Phys. Earth Plant. Inter.* **111**, 105-121, 1999.